Materials Horizons

Large Piezoelectricity in $NaNbO_3$-based Lead-free Ceramics via Tuning Oxygen Octahedral Tilt

Journal:	*Materials Horizons*
Manuscript ID	MH-COM-10-2021-001680.R1
Article Type:	Communication
Date Submitted by the Author:	23-Nov-2021
Complete List of Authors:	Wang, Lu; University of Science and Technology Beijing, Department of Physical Chemistry Qi, He; Hefei University of Technology, Gao, Botao; University of Science and Technology Beijing Liu, Ye; University of Science and Technology Beijing Liu, Hui; University of Science and Technology Beijing, Chen, Jun; University of Science and Technology Beijing, Department of Physical Chemistry

ARTICLE

Large Piezoelectricity in $NaNbO_3$-based Lead-free Ceramics via Tuning Oxygen Octahedral Tilt

Received 00th January 20xx,
Accepted 00th January 20xx

DOI: 10.1039/x0xx00000x

Lu Wang,[a,b] He Qi,*[a,b] Botao Gao,[a,b] Ye Liu,[a,b] Hui Liu[a,c] and Jun Chen* [a,b]

The development of high-performance lead-free piezoceramics for replacing Pb-based perovskites has attracted lots of attention, and comparable room-temperature piezoresponse has been realized in (Na,K)NbO_3 and $BaTiO_3$-based ceramics with local structure heterogeneity via adjusting polymorphic phase boundary. In this work, a new method of oxygen octahedron tilt design is used in $NaNbO_3$-based lead-free ceramics, which usually shows complex oxygen octahedron tilt information inherited from $NaNbO_3$. The substitution of $Ba(Fe_{0.5}Nb_{0.5})O_3$ and $BaTiO_3$ with high tolerance factor into $NaNbO_3$ leads to a gradual elimination of anti-parallel cation displacement and anti-phase tilt along three axes; as a result, a single tetragonal phase with *P4bm* space group and only in-phase tilt along *c* axis is achieved in $0.88NaNbO_3$-$0.04Ba(Fe_{0.5}Nb_{0.5})O_3$-$0.08BaTiO_3$ ceramic. Accompanying the decreased oxygen octahedral tilt degree, a drastically improved d_{33} up to 367 pC/N (over ten times that of $NaNbO_3$ ceramic) is obtained, reaching a record high in $NaNbO_3$-based lead-free ceramics. Together with temperature insensitive piezoresponse originating from thermal stable oxygen octahedral tilt structure, the studied $NaNbO_3$-based materials show large potential for replacing Pb-based ceramics in some electronic devices. The oxygen octahedron tilt engineering would be used for designing more high-performance lead-free ceramics with high piezoresponse and excellent thermal stability simultaneously.

New concepts

The origin of polarization in perovskites roots in A/B-site displacement and BO_6 octahedral tilt. The adjustment of A/B-site displacement through ions doping is widely used for realization of large piezoelectricity, yet BO_6 octahedral distortion design rarely pays attention by researchers, because the existence of oxygen octahedral tilt is widely thought to be bad for the room temperature piezoelectric response but favor of the thermal stability. In this work, $NaNbO_3$ lead-free ceramic showing high Curie temperature and complex oxygen octahedral tilt system is chosen as the matrix, a novel method of oxygen octahedral tilt engineering, including not only tilt degree but also tilt mode, is used to generate high piezoelectric properties and excellent thermal stability at the same time. With the gradual elimination of antiphase tilt along *a* and *b* axes as well as decrease of tilt degree, temperature-insensitive large d_{33}~367 pC/N is obtained in a new $0.88NaNbO_3$-$0.04Ba(Fe_{0.5}Nb_{0.5})O_3$-$0.08BaTiO_3$ ceramic. The detected d_{33} in the studied single-phase sample is much higher than that of the MPB compositions previously reported in NN-based ceramics. The results suggest that the oxygen octahedral tilt design would be a good strategy similar to polarization configuration for designing high-performance in some special lead-free ceramic systems.

Introduction

Ferroelectric and piezoelectric ceramics as functionalized materials provide engineering applications, including sensors, transducers, and energy storage devices.[1,2] In particular, piezoelectric coefficient d_{33} is an important parameter for evaluating ceramic properties.[3] The effective ways to obtain high d_{33} consist of constructing phase boundary (i.e., morphotropic phase boundary, MPB and polymorphic phase boundary, PPB),[4,5] forming relaxation state[6] and nanodomain structure.[7] Traditional Pb-based $Pb(Zr_{0.53}Ti_{0.47})O_3$ as commercial ceramic locates at MPB with rhombohedral (*R*) and tetragonal (*T*) phase, showing high piezoelectricity and temperature stability.[8] Lead-free $(Na_{0.5}K_{0.5})NbO_3$ (NKN)[9] and $BaTiO_3$ (BT)[10]-based systems exhibit PPB varying with not only composition but also temperature for superior d_{33} up to 600+pC/N.[11] Relaxor ferroelectric $Pb(Mg_{1/3}Nb_{2/3})O_3$-$PbTiO_3$ processes outstanding d_{33} ~ 680pC/N, accompanied by nanodomain morphology with easy polarization rotation.[12, 13] A large number of works through ions doping for continuously improved piezoresponse have been achieved in recent years.[14-16]

The origin of polarization in perovskite structure roots in A/B-site displacement and BO_6 octahedral distortion.[17, 18] Many pieces of research concentrate on the former to adjust the magnitude and direction of ion displacement. Generally, the existence of oxygen octahedral distortion in lead-free systems,

[a] Beijing Advanced Innovation Center for Materials Genome Engineering, University of Science and Technology Beijing, Beijing 100083, China. E-mail: qihehfut@163.com (H. Qi), junchen@ustb.edu.cn (J. Chen)
[b] Department of Physical Chemistry, University of Science and Technology Beijing, Beijing 100083, China.
[c] School of Mathematics and Physics, University of Science and Technology Beijing, Beijing 100083, China.
† Footnotes relating to the title and/or authors should appear here.
Electronic Supplementary Information (ESI) available: [details of any supplementary information available should be included here]. See DOI: 10.1039/x0xx00000x

such as $(Bi_{0.5}Na_{0.5})TiO_3$ (BNT)-based ceramics,[19-21] as a key factor restricts improvement of piezoelectric properties.[22, 23] Therefore, it is vital to understand and tune oxygen octahedral tilt in lead-free piezoelectrics design.[24, 25] Typical lead-free compound $NaNbO_3$ as classical antiferroelectrics with anti-parallel cation displacements owns abundant BO_6 distortion configuration.[26] The antiferroelectric orthorhombic phase at room temperature processes $a^-b^-c^-$ and $a^-b^-c^+$ tilting with *Pbcm* space group.[27, 28] The high temperature phases inherit its parent distortion, according to Glazer notation,[29] respectively: $a^-b^+c^+$/ $a^-b^0c^+$ (*R*), $a^-b^+c^+$ (*S*), $a^-b^0c^+$ (T_1), $a^0a^0c^+$ (T_2).[30] The substitution of the second component, including $LiNbO_3$ and $BaTiO_3$, can stabilize the ferroelectric state for achieving a high piezoelectric response.[31, 32] Besides, A-site vacancies engineering is introduced to adjust octahedral tilting.[33] Nevertheless, partial BO_6 octahedral tilting remains, like ferroelectric *Q* phase $P2_1ma$ and ferroelectric *R* phase *R3c*.[34, 35] BO_6 distortion is related to tolerance factor (*t*), which describes the competition relationship between A-O and B-O.[36, 37] Significantly, lower *t* generally is accompanied by oxygen octahedral rotation to maintain perovskite structure owing to small A-site ion radius.

In order to regulate BO_6 octahedral distortion, large *t* compounds are introduced to affect structure phase transition for exploring high-performance piezoelectric ceramics.[38] Here, large *t* composition $Ba(Fe_{0.5}Nb_{0.5})O_3$ (BFN) doping in NN leads to stabilizing ferroelectric *Q* phase, firstly. The third phase BT mixing further enlarges *t* to reduce oxygen octahedral distortion for inducing the *T* phase.[39] The composition of 0.88NN-0.04BFN-0.08BT exhibits excellent piezoelectric performance with d_{33} ~ 367 pC/N and outstanding temperature stability in the range of 20-120 °C originated from a single polar *P4bm* structure.

Experimental

The three compositions of NN, 0.96NN-0.04BFN and 0.88NN-0.04BFN-0.08BT were fabricated by a conventional solid-state reaction method. The raw materials chose Na_2CO_3 (99.8%, 497-19-8, Aladdin, Shanghai), Nb_2O_5 (99.9%, 1313-96-8, Aladdin, Shanghai), $BaCO_3$ (99.95%, 12047-27-7, Aladdin, Shanghai), Fe_2O_3 (98%, 1309-37-1, Aladdin, Shanghai), and TiO_2 (99.8%, 13463-67-7, Aladdin, Shanghai), which were calcined at 300 °C for 2 hours before mixing to remove moisture and volatile impurity. The weighed powder was mixed at a planetary ball mill to grind with alcohol for 12 hours. The dried powder was calcined at 900 °C for 4 hours and then ball-milled again for 12 hours. The resultant powder was pressed into green pellets 10 mm diameter using polyvinyl alcohol (PVA) as a binder under 300 MPa pressure. The pressed pellets were sintered in the temperature range of 1260-1350 °C for 2 hours after removing the binder at 550 °C for 2 hours. For dielectric,

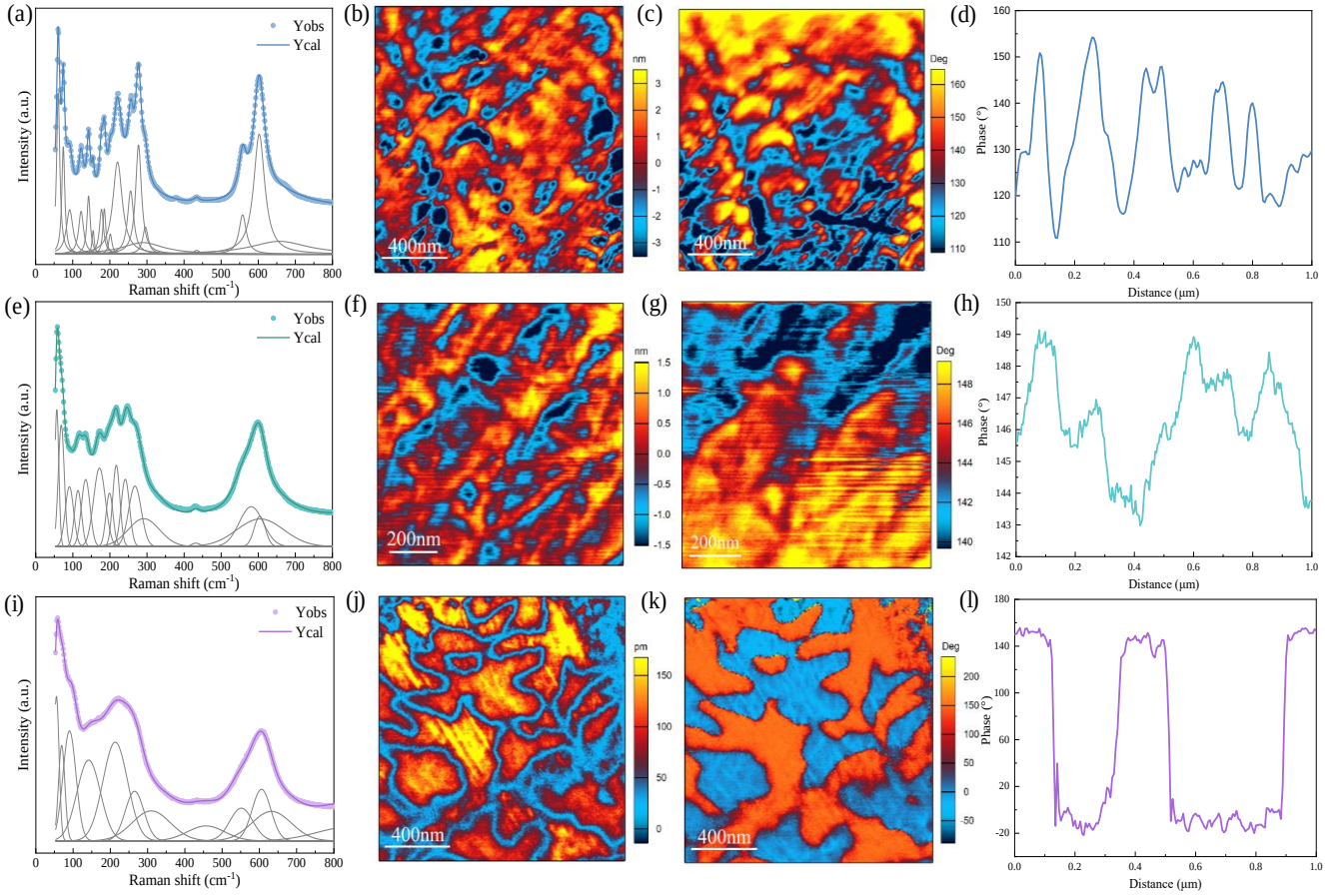

Fig. 1. The composition dependence Raman spectra and corresponding deconvolution results at 50-800 cm^{-1}, PFM amplitude and phase image, as well as phase profiles generated from the line scan of (a-d) NN, (e-h) 0.96NN-0.04BFN and (i-l) 0.88NN-0.04BFN-0.08BT ceramics.

ferroelectric and piezoelectric measurement, the as-sintered disks were polished to a thickness of ~0.6 mm with sputtering Au electrodes (ETD2000, Elaborate Technology Development, Beijing). The samples were poled with a dc electrical field of 3-12 kV/mm at room temperature for 30 minutes in a silicone oil bath. Dielectric curves under different temperatures and frequencies were measured with an LCR meter (E4980, Agilent, Santa Clara, CA) under 0.5 V at various frequencies. The ferroelectric properties, including polarization and bipolar strain curves versus the electric field, were measured using a ferroelectric analyzer (aixACCT, TF Analyzer 1000, Aachen, Germany) at 1.5 Hz under an electric field of 12 kV/mm, 6 kV/mm and 3 kV/mm, respectively. The piezoelectric coefficient d_{33} was measured using a quasi-static d_{33} meter (China Academy of Acoustics, ZJ-3, Shanghai). The remnant d_{33} values were measured at room temperature after annealing at different temperatures for 30 minutes.

The powder neutron diffraction data were collected at CSNS (China Spallation Neutron Source, MPI) using time-of-flight powder diffractometers. Rietveld refinements were performed using GSAS 2. Room-temperature high energy synchrotron X-ray diffraction (SXRD) with different compositions was measured at the beamline 11-ID-C in Advanced Photon Source (APS) with λ = 0.1173Å. High-temperature SXRD was collected at the beamline 17-BM of APS with high-energy X-ray radiation (λ = 0.24105 Å) in the range of 25-150 °C. The Raman spectra in the range of 50-800 cm^{-1} were collected at room temperature using a Raman spectrometer (HR Evolution, Horiba, France). The grain morphology and size were observed in as-sintered ceramics surface by field-emission scanning electron microscope ((FE-SEM; LEO1530, ZEISS SUPRA 55, Oberkochen, Germany). The domain structure results were proofed by piezoresponse force microscope (PFM) using an atomic force microscope (MFP-3D, Asylum Research, USA), using in-plane and out-of-plane mode with single frequency tracking under 8 V testing voltage. The measured PFM samples were polished after rubbing under 2000–7000 mesh sandpapers without obvious scratches under 3000 times optical microphotograph. The domain morphology observation and selected area electron diffraction (SAED) were performed on a field-emission transmission electron microscope (FE-TEM; JEM-2200FS, JEOL, Japan) operated at 200 kV. For TEM examination, samples were first mechanically polished to a thickness of ~20 μm, then ion-milled on a Precision Ion Polishing System (PIPS, Model 695, Gatan Inc., Pleasanton, CA, USA) at 5 keV.

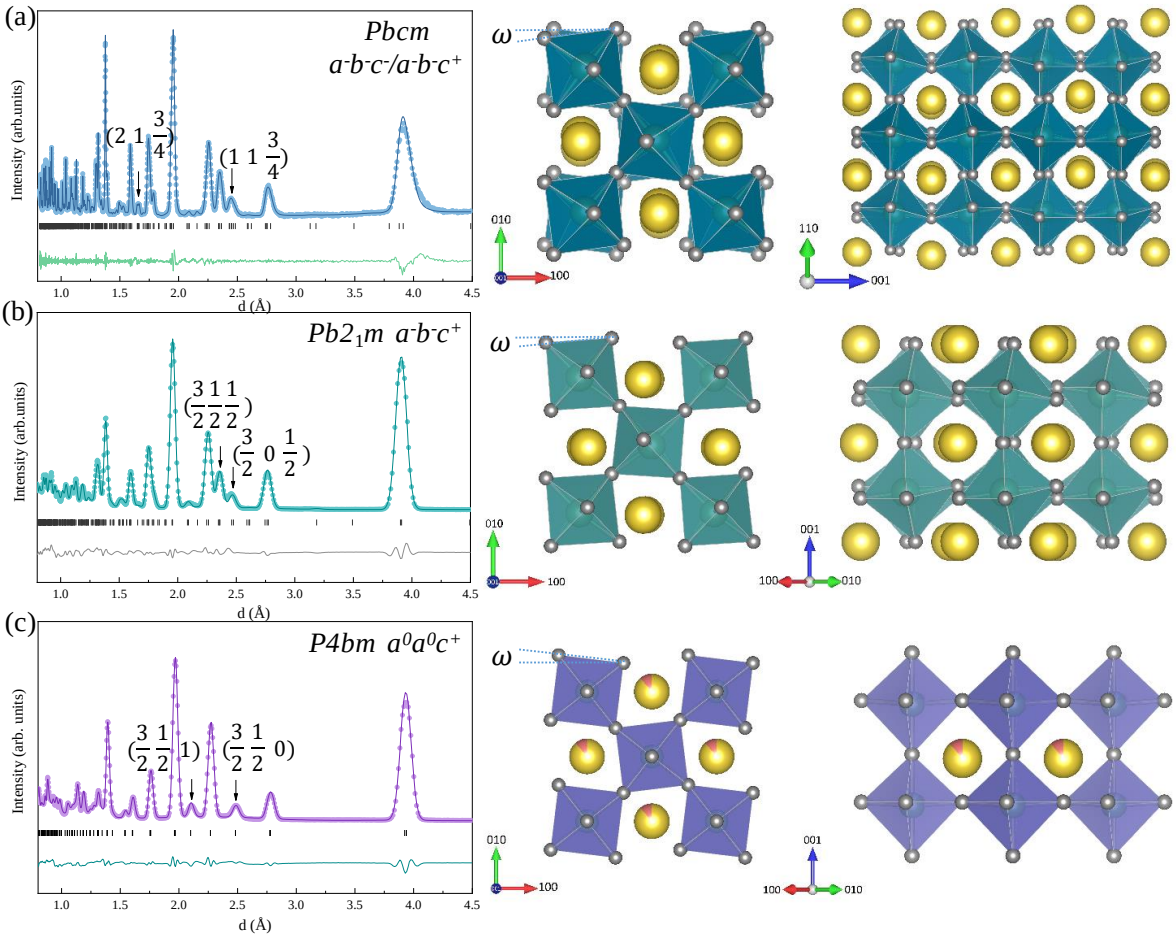

Fig. 2. The Rietveld refinement result of powder neutron diffraction as well as the achieved crystal structure diagram for (a) NN, (b) 0.96NN-0.04BFN and (c) 0.88NN-0.04BFN-0.08BT ceramics.

Results and discussion

NN as the initial phase is chosen not only for its complex octahedral configuration but also a variable structure phase transition with changing the ambinent temperature, indicating a sensitive response of tilting. For the stabilization of ferroelectric phase, the substitution composition needs large *t* meaning large radius A-site cation, such as Ba^{2+} (r_{Ba} = 0.161 nm, r_{Na} = 0.139 nm). Thus, $Ba(Fe_{0.5}Nb_{0.5})O_3$ with same B-site ion Nb^{5+} (r_{Nb} = 0.064 nm) and balanced valence Fe^{3+} (r_{Fe} = 0.065 nm) ion own large t ~ 1.0421 doping in NN matrix. Subsequently, $BaTiO_3$ with greater t ~ 1.0615 is chosen for further modification. The composition-dependent high-energy synchrotron X-ray diffraction (SXRD) patterns in Fig. S1 present pure perovskite structure without secondary phases. An obvious change in the symmetry can be detected according to the magnified $\{004\}_C$ diffraction peaks as well as Raman peaks shown in Fig. S1 and Fig. 1, respectively. As known, pure NN exhibits antiferroelectric P phase with *Pbcm* space group and orthorhombic symmetry at room temperature, which originates from the anti-parallel displacement of Nb in a direction along one diagonal in the plane of the O3-O4 square as well as off-centering displacement of Na2 (Na1 remains almost undisplaced).[40, 41] As a result, several typical features such as I_{004}/I_{400} = 2:1, superlattice diffractions in the range of 2θ = 6.8 ~ 7.0° and multiple Raman peaks at < 300 cm^{-1} can be seen. With the substitution of 4 mol% BFN for NN, an orthorhombic structure can also be identified according to the feature of I_{004}/I_{400} = 2:1. However, the obvious change of the space group can be confirmed by the obvious decreased number of Raman peaks. On the one hand, the split Raman peaks at ~75 cm^{-1} merge, indicating the absence of the off-centering displacement of Na2 found in the P phase. On the other hand, the decreased number of Raman peaks caused by the internal vibrational modes of the NbO_6 octahedron suggests the disappearance of the B-site cation anti-parallel displacement feature. Therefore, a ferroelectric orthorhombic phase has been stabilized at room temperature for 0.96NN-0.04BFN, which would be unstable and might turn back to the antiferroelectric phase on heating to 230 °C, as can be seen by the significant dielectric anomaly shown in Fig. S2. After the addition of BT into 0.96NN-0.04BFN, a tetragonal phase can be identified. Moreover, broadened Raman peaks suggest the increased compositional disorder, further reflected on the weak dielectric relaxation behavior.

The evolution of structural symmetry and ferroelectricity would also be reflected in the change of domain structure. The domain morphology and polarization switching at the microscopic scale can be provided in PFM patterns. All the studied samples exhibit dense structure and uniform size without abnormally grown grains (Fig. S3). The grain size difference is mainly attributed to the optimized sintering temperature and variable element types, changing from 1350 °C in NN, 1280 °C in 0.96NN-0.04BFN, to 1240 °C in 0.88NN-0.04BFN-0.08BT. The in-plane PFM amplitude and phase signal of NN shown in Figs. 1(b,c) display regular bulk nanodomain with a width less than 100 nm. Even though an antiferroelectric P phase is usually identified for pure NN ceramic at room temperature, weak ferroelectricity can be usually detected owing to the similar free

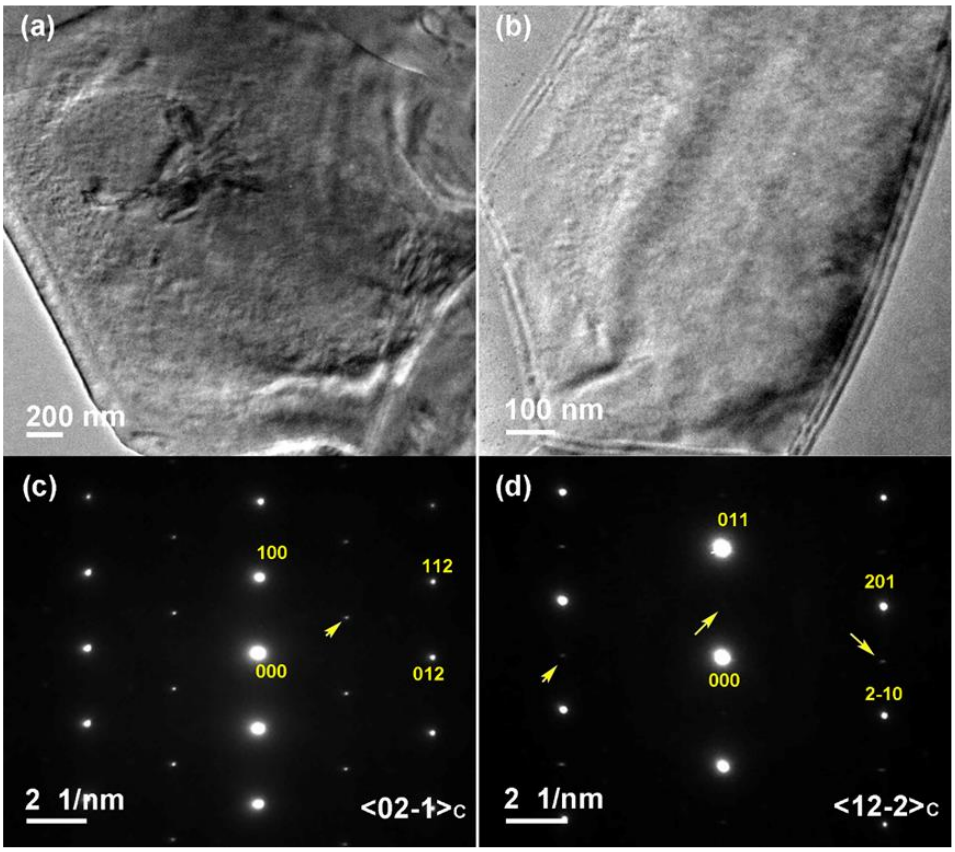

Fig. 3. (a,b) Bright-field TEM images and (c,d) SAED of 0.88NN-0.04BFN-0.08BT ceramic.

energy of P phase to the ferroelectric Q phase. With the stabilization of the ferroelectric Q phase, the 0.96NN-0.04BFN exhibits enlarged stripe-like domains in Figs. 1(f,g). Normal ferroelectric ceramics with tetragonal phase usually exhibit large stripe domains, yet irregular domains can be seen in the 0.88NN-0.04BFN-0.08BT sample, as shown in Figs. 1(j,k). This should be related to the broken long-range ordering in relaxor ferroelectrics. The corresponding phase profiles generated from the line scan are provided in Figs. 1(d,h,l) to observe the domain size variation directly. Both processes of enhanced ferroelectricity and refined domains would be in favor of the piezoelectric response. In addition, the corresponding surface topography shown in Fig. S4 eliminates the influence of morphology fluctuation on domain configuration.

Besides the ferroelectricity reflected on phase structure, lattice distortion relating to the cation off-centering displacement and domain size, oxygen octahedral tilt also plays important roles in piezoelectric properties. In most high-performance perovskite piezoceramics, the polarization heterogeneity has been designed at average or local scale.[14, 42, 43] The contribution of oxygen octahedral tilt on piezoelectric properties is usually ignored, even many pieces of research suggest that the existence of oxygen octahedral tilt is bad for the piezoresponse.[38, 44] Yet, the oxygen octahedral tilt information is non-ignorable in NN-based lead-free ceramic owing to the inheritance from the

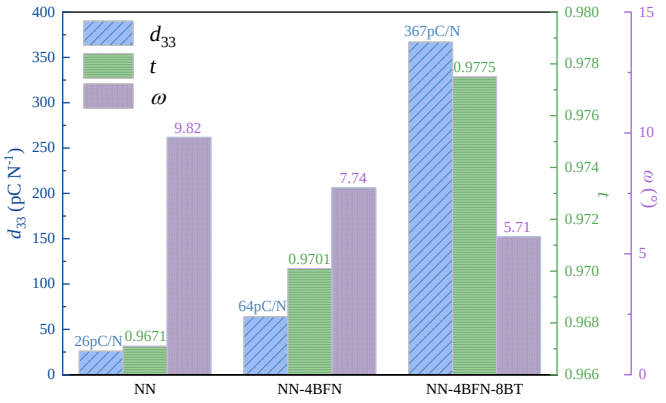

Fig. 4. The composition dependence for small signal piezoelectric coefficient (d_{33}), tolerance factor (t) and octahedral distortion angle (ω).

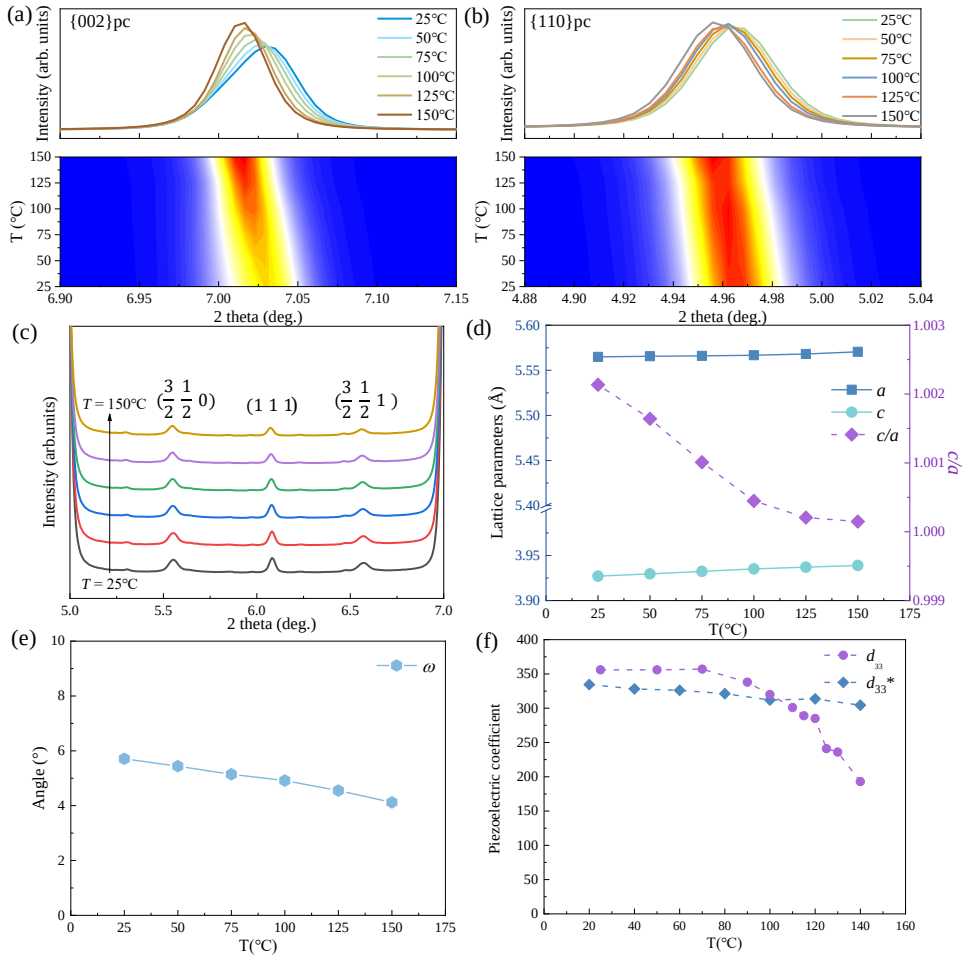

Fig. 5. (a,b) Diffraction peak profiles and contour plots of *{110}*$_C$ and *{002}*$_C$, (c) enlarged superstructure diffraction peaks in the temperature range of 25-150 °C, (d,e) lattice parameters, axial ratio and angle ω of distortion as the function of temperature, (f) temperature dependent d_{33} and d_{33}^* for the 0.88NN-0.04BFN-0.08BT ceramic.

complex oxygen octahedral tilt of NN. In order to get the accurate oxygen octahedron tilting information, the room-temperature powder neutron diffraction was taken, and the Rietveld refinement results are shown in Fig. 2 and Table S1. The structural refinement confirms that NN ceramic exhibits orthorhombic phase with *Pbcm* space group,[25, 26] which owns a complex combination oxygen octahedron tilt of $a^-b^-c^-$ and $a^-b^-c^+$ (equivalent to $(a^-a^-c^-)/(a^-a^-c^+)$ owing to $b^- = a^-$), especially repeat units of $c^+c^+c^-c^-$ along *c* axis, leading to a supercell with $\sqrt{2}a_p \times \sqrt{2}a_p \times 4a_p$ (a = 5.5040Å, b =5.5689Å, c =15.5194Å) by comparing with basic perovskite cubic lattice of a_p~3.9 Å.

With the substitution of BFN, ferroelectric Q phase with $Pb2_1m$ space group and $a^-b^-c^+$ oxygen octahedron tilt can be identified.[45] By comparing with NN, the anti-phase tilt along *c* axis and anti-parallel displacement of B-site cations disappears, resulting in the absence of $\{1\ 1\ 3/4\}_C$ and $\{2\ 1\ 3/4\}_C$ superlattice diffraction peaks.[46] According to the systematic research results from *A.M. Glazer*, in-phase tilt and anti-phase tilt would produce *1/2(ooe)* (*o*: odd and *e*: even) and *1/2*(*ooo*) superlattice diffraction peaks, respectively.[47] Therefore, some *1/2* type superlattice diffractions can still be detected in the reciprocal space, including $(3/2\ 1/2\ 1/2)_C$ and $(3/2\ 0\ 1/2)_C$ as shown in Fig. 2(b).[34] With further adding BT, a tetragonal phase with $a_p = b_p < c_p$ can be achieved, this leaves $a^0a^0c^+$ and $a^0a^0c^-$ as the only possible tilt systems. By further looking into the superlattice diffraction peaks, *1/2*(*ooe*) instead of *1/2*(*ooo*) can be seen, eliminating $a^0a^0c^-$. Thus the 0.88NN-0.04BFN-0.08BT ceramic should belong to a *P4bm* phase with $a^0a^0c^+$ tilt, and the anti-phase tilt has been eliminated after BT adding.[23] The superlattice diffraction can also be measured by TEM, as shown in Fig. 3 for the 0.88NN-0.04BFN-0.08BT ceramic. Nanodomains with weak contrast instead of stripe-like micro-domains can be seen. Moreover, obvious *1/2*(*ooe*) superlattice spots can be detected on the SAED patterns, confirming the Rietveld refinement results of neutron powder diffraction.

The oxygen octahedron tilt is thought to be dependent on *t*, a quantity suggested by *Goldschmidt* to determine the stability of perovskite phases:

$$t=(R_A+R_O)/[2^{1/2}(R_B+R_O)]$$

R_A, R_B and R_O are the radii of the A- and B-site cations and the O ion, respectively.[48, 49] The occurrence of tilt would reduce the interstice volume and improve the structure stability when *t* decreases below 0.985.[37] NN exhibits a relatively low t ~ 0.9671 to maintain the perovskite structure, anti-phase and in-phase tilt, as well as anti-parallel cation displacement occur simultaneously. This structure is quite stable under external stimulation such as electric field and stress; thus a high driving field (~10 kV/mm, see Fig. S5) and poor piezoelectric properties (d_{33} ~ 26 pC/N) can be measured. Adding BFN with a higher t ~ 1.0421 would decrease the tilt degree, eliminating the c^- tilt in NN. In order to quantitatively analyze the change of tilt degree, the oxygen octahedron distortion angle ω, which is calculated by the inclination of O-O-O atoms, displays raised angle approaching zero with distortion-free structure caused by the in-phase tilt is given. This is because the in-phase tilt exists in these three structures and only exists along *c* axis, as clearly shown in Fig. 2. The ω value decreases from 9.82° to 7.74° with the substitution of 4 mol% BFN for NN, while the d_{33} value is twice as much as that of NN ceramic, as shown in Fig. 4. Accompanying the further elimination of anti-phase tilt along *a* and *b* axes with substituting BT, a further decreased ω value of ~5.71° can be obtained. The gradually decreased lattice distortion makes the domain switching behavior easier, as reflected in the decreased coercive electric field (Fig. S5). Most importantly, a drastically enhanced piezoresponse with d_{33} ~ 367 pC/N is realized, reaching a record high of NN-based lead-free ceramics. A design of oxygen octahedral tilt, including not only tilt degree but also tilt mode as changing *t* can be observed. The distortion along the *c* axis remains regardless of the space group defined as distortion angle ω to evaluate the degree of distortion, which gradually decreases with enhancing *t*. Meanwhile, tilt mode transforms from tilt along three axes in NN to two axes in 0.96NN-0.04BFN, and final only *c* axis in 0.88NN-0.04BFN-0.08BT, which means the change from tilt to tilt-free along some directions, accompanying with the evolution of phase structure. A net dipole moment of polarization is the origin of ferroelectricity.[17] The polarization rotation and polarization extension as a mechanism directly affect the piezoelectric response. Importantly, polarization rotation is the dominant factor for d_{33} in rotator ferroelectrics.[50, 51] The existence of oxygen octahedral tilt leads to a large energy barrier, which inhibits polarization rotation under electric field. Meanwhile, the greater the octahedral distortion degree, the higher the energy barrier of polarization rotation. The inhibited polarization switching ability leads to inferior piezoelectricity.[38] In the classical BNT-BT system, the decreased oxygen octahedral tilting also exits with increasing BT content, transforming from tilting to untilting structure: *R3c* in BNT to *P4bm* in BNT-7BT, *P4mm* in BNT-10BT.[52] The suppressed d_{33} is mainly *R3c-P4mm* or *R3c-P4bm* phase boundary with tilt oxygen octahedral configuration.[53] If this tilting can be avoided, such as forming a *R3m-P4mm* phase boundary similar to that of PZT-based ceramics, the piezoelectric performance will be improved in qualitative change.

The room temperature d_{33} of the studied NN-based ceramic is much larger than that of BNT-based[54] lead-free ceramics and slightly inferior to that of NKN and BT-based lead-free ceramics. However, the ultrahigh piezoelectric response in NKN[55] and BT[56]-based lead-free ceramics is commonly achieved through shifting the polymorphic phase transition temperature to room temperature, leading to the sacrifice of thermal stability simultaneously. Moreover, the moisture absorption and volatilization of potassium and the low Curie temperature of BT also limit the usage of NKN and BT in the industry. Differently, NN-based piezoelectric ceramics usually exhibit excellent temperature stability, no matter for the samples with single-phase or MPB.[57] This should be ascribed to the existence of oxygen octahedral tilt, which is usually quite insensitive to temperature change compared with PPB. The lattice distortion evolution can be obtained from the Rietveld refinement of the high-energy SXRD results measured under various temperatures, as shown in Figs. 5, S6 and Table S2. Even though the *c*/*a* decreases gradually on heating, the *P4bm* structure keeps quite stable up to T_C ~ 150°C, as can be reflected on the existence of

(3/2 1/2 0)$_C$ and *(3/2 1/2 1)*$_C$ superlattice diffraction peaks in Fig. 5(c).[58] The calculated oxygen octahedral distortion angle ω exhibits minor variation from 5.7° to 4° when heating from room temperature to 150 °C, providing the basis of temperature-insensitive piezoelectric and ferroelectric properties (Figs. 5(e,f)). The large-signal d_{33}^* calculated from temperature-dependent unipolar strain in Fig. S7 exhibits a maximum up to 331 pm/V at ~ 20 °C and then sightly decreases, culminating in stabilizing 320 pm/V. In comparison, the small-signal d_{33} owns large piezoelectricity up to 367 pC/N and outstanding temperature stability at 20-120 °C.

Conclusions

In conclusion, the evolution of phase structure, oxygen octahedral distortion, domain morphology, ferroelectric and piezoelectric performance for NN, 0.96NN-0.04BFN, and 0.88NN-0.04BFN-0.08BT lead-free ceramics are systematically researched in this work. The oxygen octahedral tilt (both tilt mode and tilt degree) design was done to prepare a novel NN-based ceramic with a single phase instead of an MPB by fine compositional tuning. The enlarged *t* leads to a gradual phase transition from antiferroelectric orthorhombic with *Pbcm* space group to ferroelectric orthorhombic with $Pb2_1m$ space group and then to ferroelectric tetragonal with *P4bm* space group, accompanying a gradual elimination of anti-phase tilt of oxygen octahedron. The decreased oxygen octahedral tilt degree and improved piezoelectric and ferroelectric properties have been obtained in the novel 0.88NN-0.04BFN-0.08BT ceramic. Especially, a large d_{33} ~ 367 pC/N reaching a record high of NN-based lead-free ceramic is achieved via the design of oxygen octahedral tilt, which also exhibits excellent temperature stability in the range of 20-120 °C owing to the stable oxygen octahedral tilt of *P4bm* single phase. The oxygen octahedral tilt engineering found in this work would provide a new method for designing high-performance lead-free ceramics with temperature-insensitive large piezoresponse.

Author Contributions

J. C., H. Q and L. W. designed the research. L. W., Y. L. and H. Q prepared the samples and took the measurements of the macroscopic electric properties. H. L. and B. G. performed the *in situ* high-energy synchrotron X-ray diffraction experiment. L. W. and Y. L. performed the TEM experiments. L. W. and H. Q. analyzed TEM data. L. W. and B. G. collected the neutron diffraction data. L. W., H. Q. and H. L. analyzed the diffraction data. L. W., H. Q. and J. C. wrote the manuscript, with contributions from the other authors. J. C. and H. Q. guided the projects.

Conflicts of interest

There are no conflicts to declare.

Acknowledgements

This work was supported by the National Natural Science Foundation of China (Grant Nos. 21825102, 52172181, and 22105017), the Fundamental Research Funds for the Central Universities, China (Grant No. 06500186), the China Postdoctoral Science Foundation (Grant Nos. 2020M680345 and 2021T140048). This research was used resources of the China Spallation Neutron Source and the Advanced Photon Source, a US Department of Energy (DOE) Office of Science User Facility operated for the DOE Office of Science by Argonne National Laboratory under Contract No. DE-AC02-06CH11357.

Notes and references

1 K. Uchino, *Smart Mater. Struct.*, 1998, **7**, 273-285.
2 T. R. Gururaja, W. A. Schulze, L. E. Cross and R. E. Newnham, *IEEE Trans. Sonics Ultrason.*, 1985, **32**, 499-513.
3 M. D. Maeder, D. Damjanovic, N. Setter, *J. Electroceram.* **2004**, 13.
4 W. Cao and L. E. Cross, *Phys. Rev. B*, 1993, **47**, 4825-4830.
5 Y. Dai, X. Zhang and G. Zhou, *Appl. Phys. Lett.*, 2007, **90**, 262903.
6 V. V. Shvartsman, D. C. Lupascu and D. J. Green, *J. Am. Ceram. Soc.*, 2012, **95**, 1-26.
7 R. Theissmann, L. A. Schmitt, J. Kling, R. Schierholz, K. A. Schönau, H. Fuess, M. Knapp, H. Kungl and M. J. Hoffmann, *J. Appl. Phys.*, 2007, **102**, 024111.
8 H. Jaffe, W. R. Cook Jr, B. Jaffe, *Academic Press*, 1971, **317**, 562-563.
9 Y. Saito, H. Takao, T. Tani, T. Nonoyama, K. Takatori, T. Homma, T. Nagaya and M. Nakamura, *Nature*, 2004, **432**, 84-87.
10 W. Liu and X. Ren, *Phys. Rev. Lett.*, 2009, **103**, 257602.
11 J. Fu and R. Zuo, *Acta Mater.*, 2020, **195**, 571-578.
12 B. Noheda, D. E. Cox, G. Shirane, J. Gao and Z. G. Ye, *Phys. Rev. B*, 2002, **66**, 054104.
13 H. Wang, J. Zhu, X. W. Zhang, Y. X. Tang and H. S. Luo, *J. Am. Ceram. Soc.*, 2008, **91**, 2382-2384.
14 F. Li, D. Lin, Z. Chen, Z. Cheng, J. Wang, C. Li, Z. Xu, Q. Huang, X. Liao, L. Q. Chen, T. R. Shrout and S. Zhang, *Nat Mater*, 2018, **17**, 349-354.
15 T. Zheng, H. Wu, Y. Yuan, X. Lv, Q. Li, T. Men, C. Zhao, D. Xiao, J. Wu, K. Wang, J.-F. Li, Y. Gu, J. Zhu and S. J. Pennycook, *Energy Environ. Sci.*, 2017, **10**, 528-537.
16 H. Tao, H. Wu, Y. Liu, Y. Zhang, J. Wu, F. Li, X. Lyu, C. Zhao, D. Xiao, J. Zhu and S. J. Pennycook, *J. Am. Chem. Soc.*, 2019, **141**, 13987-13994.
17 R. E. Cohen, *Nature*, 1992, **358**, 136-138.
18 S. C. Abrahams, S. K. Kurtz and P. B. Jamieson, *Phys. Rev.*, 1968, **172**, 551-553.
19 H. Qi and R. Zuo, *J. Mater. Chem. A*, 2019, **7**, 3971-3978.
20 T. Rojac, A. Bencan, B. Malic, G. Tutuncu, J. L. Jones, J. E. Daniels, D. Damjanovic and D. J. Green, *J. Am. Ceram. Soc.*, 2014, **97**, 1993-2011.
21 I. Levin, I. M. Reaney, E. M. Anton, W. Jo, J. Rödel, J. Pokorny, L. A. Schmitt, H. J. Kleebe, M. Hinterstein and J. L. Jones, *Phys. Rev. B*, 2013, **87**, 024113.
22 G. O. Jones and P. A. Thomas, *Acta Cryst.*, 2002, **58**, 168-178.
23 C. Ma, H. Guo, S. P. Beckman and X. Tan, *Phys. Rev. Lett.*, 2012, **109**, 107602.
24 H. Luo, H. Liu, S. Deng, S. Hu, L. Wang, B. Gao, S. Sun, Y. Ren, L. Qiao and J. Chen, *Acta Mater.*, 2021, **208**, 116711.
25 H. Liu, Z. Zhou, Y. Qiu, B. Gao, S. Sun, K. Lin, L. Ding, Q. Li, Y. Cao, Y. Ren, J. Sun, X. Xing and J. Chen, *Mater. Horiz.*, 2020, **7**, 1912-1918.
26 J. Chen and D. Feng, *Phys. Status Solidi A*, 1988, **109**, 171-185.

27 K. E. Johnston, C. C. Tang, J. E. Parker, K. S. Knight, P. Lightfoot and S. E. Ashbrook, *J. Am. Chem. Soc.*, 2010, **132**, 8732-8746.
28 M. Yashima, S. Matsuyama, R. Sano, M. Itoh, K. Tsuda and D. Fu, *Chem. Mater.*, 2011, **23**, 1643-1645.
29 A. Glazer, *Acta Cryst.*, 1972, **B28**, 3384-3392.
30 S. K. Mishra, N. Choudhury, S. L. Chaplot, P. S. R. Krishna and R. Mittal, *Phys. Rev. B*, 2007, **76**, 024110.
31 S. K. Mishra, P. S. R. Krishna, A. B. Shinde, V. B. Jayakrishnan, R. Mittal, P. U. Sastry and S. L. Chaplot, *J. Appl. Phys.*, 2015, **118**, 094101.
32 J. T. Zeng, K. W. Kwok and H. L. W. Chan, *J. Am. Ceram. Soc.*, 2006, **89**,2828-2832.
33 I. Levin, F. Yang, R. Maier, W. J. Laws, D. S. Keeble, G. Cibin and D. C. Sinclair, *Adv. Funct. Mater.*, 2020, **30**, 2001840.
34 Y. I. Yuzyuk, E. Gagarina, P. Simon, L. A. Reznitchenko, L. Hennet and D. Thiaudière, *Phys. Rev. B*, 2004, **69**, 144105.
35 H. Qi, A. Xie, J. Fu and R. Zuo, *Acta Mater.*, 2021, **208**, 116710.
36 I. Grinberg and A. M. Rappe, *Phase Transitions*, 2011, **80**, 351-368.
37 I. M. Reaney, E. L. Colla and N. Setter, *Jpn. J. Appl. Phys.*, 1994, **33**, 3984-3990.
38 K. Yan, S. Ren, M. Fang and X. Ren, *Acta Mater.*, 2017, **134**, 195-202.
39 L. Gacem, D. Ouadjaout, J.-P. Chaminade, M. Maglione, R. Von der Mühll and S. Pechev, *Mater. Res. Bull.*, 2009, **44**, 2240-2245.
40 I. Levin, V. Krayzman, J. C. Woicik, J. Karapetrova, T. Proffen, M. G. Tucker and I. M. Reaney, *Phys. Rev. B*, 2009, **79**, 104113.
41 C. A. Randall, Z. Fan, I. Reaney, L. Q. Chen and S. Trolier‐McKinstry, *J. Am. Ceram. Soc.*, 2021, **104**, 3775-3810.
42 F. Li, S. Zhang, D. Damjanovic, L. Q. Chen and T. R. Shrout, *Adv. Funct. Mater.*, 2018, **28**, 1801504.
43 T. Zheng and J. Wu, *Mater. Horiz.*, 2020, **7**, 3011-3020.
44 J. Fu, H. Qi, A. Xie, A. Tian and R. Zuo, *Acta Mater.*, 2021, **215**, 117100.
45 H. Guo, H. Shimizu, Y. Mizuno and C. A. Randall, *J. Appl. Phys.*, 2015, **117**, 214103.
46 H. Shimizu, H. Guo, S. E. Reyes-Lillo, Y. Mizuno, K. M. Rabe and C. A. Randall, *Dalton Trans*, 2015, **44**, 10763-10772.
47 D. I. Woodward and I. M. Reaney, *Acta Cryst.*, 2005, **B61**, 387-399.
48 R. Shannon, *Acta Cryst.*, 1976, **A32**, 751-76.
49 T. Shi, G. Li and J. Zhu, *Ceram. Int.*, 2017, **43**, 2910-2917.
50 M. Davis, M. Budimir, D. Damjanovic and N. Setter, *J. Appl. Phys.*, 2007, **101**, 054112.
51 D. Damjanovic, *Appl. Phys. Lett.*, 2010, **97**, 062906.
52 R. R. McQuade and M. R. Dolgos, *J. Solid State Chem.*, 2016, **242**, 140-147.
53 K. Yan, S. Ren, F. Wang, D. Wu, K. Zhu and X. Ren, *J. Appl. Phys.*, 2020, **127**, 164101.
54 J. Wu, in *Advances in Lead-Free Piezoelectric Materials*, 2018, pp. 191-245.
55 J.-F. Li, K. Wang, F.-Y. Zhu, L.-Q. Cheng, F.-Z. Yao and D. J. Green, *J. Am. Ceram. Soc.*, 2013, **96**, 3677-3696.
56 M. Acosta, N. Novak, V. Rojas, S. Patel, R. Vaish, J. Koruza, G. A. Rossetti and J. Rödel, *Appl. Phys. Rev.*, 2017, **4**, 041305.
57 H. Qi, R. Zuo, J.-f. Li and L. Li, *J. Eur. Ceram. Soc.*, 2018, **38**, 5341-5347.
58 L. Wang, S. Sun, H. Luo, Y. Ren, H. Liu, X. Xing and J. Chen, *J. Mater. Chem. A*, 2021, **9**, 2367-2374.